International Journal of Heat and Mass Transfer 196 (2022) 123163

Contents lists available at ScienceDirect

International Journal of Heat and Mass Transfer

journal homepage: www.elsevier.com/locate/hmt

Diffusion and reaction in a two-dimensional multilayer body: Analytical solution and imaginary eigenvalue analysis

Girish Krishnan, Ankur Jain*

Mechanical and Aerospace Engineering Department, University of Texas at Arlington, Arlington, TX, USA

ARTICLE INFO

Article history:
Received 24 February 2022
Revised 6 June 2022
Accepted 15 June 2022

Keywords:
Diffusion
Reaction
Thermal Transport
Li-ion Cell
Thermal Runaway
Imaginary Eigenvalues

ABSTRACT

Heat and mass transfer in multilayer bodies occur commonly in a number of engineering problems, such as thermal management, manufacturing and reacting systems. Much of the past literature on theoretical analysis of multilayer diffusion-reaction problems is based on the assumption of one-dimensional transport. Given the geometrical complexity of practical engineering systems, two- or three-dimensional analysis may be needed for improved accuracy. This work presents theoretical analysis of coupled diffusion and reaction occurring in a general, two-dimensional multilayer body. The transient temperature distribution is written in the form of an infinite series, and the eigenequation for this problem is derived. Adiabatic or isothermal conditions along the side walls are accounted for by appropriate choice of eigenvalues in that direction. Results are shown to be in good agreement with numerical simulations. It is shown that the temperature distribution may converge or diverge, depending on the specific values of various problem parameters, such as reaction coefficients and diffusivities in each layer, as well as the nature of the boundary conditions in both directions. An analysis for the existence of imaginary eigenvalues, which are related to divergence at large times is presented. The theoretical model is used to predict the limits of design parameters to prevent thermal runaway in a two-layer Li-ion cell. This work improves upon the limited past work on multi-dimensional multilayer transport by accounting for the reaction term, and by identifying the possibility of imaginary eigenvalues in such problems. Due to the close relationship between imaginary eigenvalues and thermal runaway, these results may contribute towards improved safety and reliability of practical engineering systems.

1. Introduction

Thermal conduction in multilayer bodies is a well-researched problem, with applications in a variety of engineering and biomedical disciplines, such as microelectronics thermal management [1], atmospheric re-entry [2] and bioheat transfer [3]. Applications for equivalent mass transport problems exist in drug delivery [4], contaminant transport [5] and chemical reactors [6]. The simplest type of such problems comprises diffusion in a one-dimensional multilayer body, such as a multilayer microelectronic device [1]. In other more complicated problems commonly referred to as Convection-Diffusion-Reaction (CDR) problems [7], convection and/or reaction also occur in addition to diffusion.

Pure-diffusion multilayer problems are solved most commonly using the method of separation of variables [8,9], although other methods such as Laplace transforms [10] and Green's functions [11] have also been used. Other, more complicated multilayer problems have also been solved, including two- and three-dimensional pure-diffusion problems [12–14], problems with advection and/or reaction in addition to diffusion [7,15] and problems with time-dependent [16] or spatially varying [17,18] boundary conditions. Literature pertaining to such problems is available in all three major coordinate systems – Cartesian, cylindrical and spherical.

In general, multilayer heat transfer problems are solved by expressing the temperature field in each layer as an infinite series, then using the boundary and interface conditions to develop relationships between coefficients of each layer and derive an eigenequation to determine a single set of eigenvalues for all layers in the problem. Quasi-orthogonality of eigenfunctions is then used to determine the last remaining coefficient [9]. While quasi-orthogonality for simple, pure-diffusion problems is very similar to a single-layer problem [8,9], introduction of advection makes this much more complicated, in both Cartesian [7] and cylindrical [4] coordinate systems.

In the past, solutions for the diffusion-reaction [15] and convection-diffusion-reaction [7] problems in a Cartesian one-dimensional multilayer body have been presented. Similar problems involving diffusion-reaction in a cylindrical/spherical body,

* Corresponding author at: 500 W First St, Rm 211, Arlington, TX, USA 76019.
E-mail address: jaina@uta.edu (A. Jain).

https://doi.org/10.1016/j.ijheatmasstransfer.2022.123163
0017-9310/

Nomenclature

Bi	Biot number, $Bi = \frac{hx_M}{k_M}$
h	convective heat transfer coefficient ($Wm^{-2}K^{-1}$)
k	thermal conductivity ($Wm^{-1}K^{-1}$)
$\bar{k}$	non-dimensional thermal conductivity, $\bar{k}_m = \frac{k_m}{k_M}$
M	number of layers
T	temperature rise about ambient (K)
t	time (s)
w	width of the body in the y direction (m)
$\bar{w}$	non-dimensional width of the body in the y direction, $\bar{w} = \frac{w}{x_M}$
x, y	spatial coordinates (m)
α	diffusivity (m^2s^{-1})
$\bar{\alpha}$	non-dimensional diffusivity, $\bar{\alpha}_m = \frac{\alpha_m}{\alpha_M}$
β	reaction coefficient (s^{-1})
$\bar{\beta}$	non-dimensional reaction coefficient, $\bar{\beta}_m = \frac{\beta_m x_M^2}{\alpha_M}$
η, ξ	non-dimensional spatial coordinates, $\eta = \frac{y}{x_M}$; $\xi = \frac{x}{x_M}$
ε	non-dimensional eigenvalue in η direction
γ	non-dimensional interface location, $\gamma_m = \frac{x_m}{x_M}$
τ	non-dimensional time, $\tau = \frac{\alpha_M t}{x_M^2}$
θ	non-dimensional temperature, $\theta_m = \frac{T_m}{T_{ref}}$
λ	non-dimensional eigenvalue in ξ direction

Subscripts

A	$x = 0$ boundary
B	$x = x_M$ boundary
in	initial temperature
m	layer number
M	total number of layers
ref	reference

with application in drug delivery from a capsule [19] or arterial balloon [4] have also been presented. Under certain conditions, these papers predict the occurrence of imaginary eigenvalues, which have been shown to be related to thermal runaway, or divergence of the temperature field at large times. Most of such past work, however, is limited to one-dimensional analysis, which, while reasonable in many practical problems, is certainly not universally valid. Due to the geometries encountered in practical problems, a two- or three-dimensional analysis may be necessitated. However, only very limited work on multilayer multidimensional conduction [12–14] is available. Such work only considers diffusion, and does not account for the reaction term, which is integral to problems such as thermal runaway in Li-ion cells and reacting systems.

It is, therefore, important to carry out theoretical analysis of thermal transport in a multidimensional multilayer problem that accounts for both diffusion and reaction. A theoretical motivation for such problem stems from the possible existence of imaginary eigenvalues in such problems. The existence of imaginary eigenvalues has been predicted for both 1D diffusion-reaction problems [5], as well as multidimensional diffusion problems [12–14]. Therefore, it is of interest to analyze the existence of imaginary eigenvalues in multidimensional multilayer diffusion-reaction problems. In addition to the theoretical novelty, there is also practical interest in imaginary eigenvalues, since the appearance of imaginary eigenvalues can be used to predict thermal runaway in systems such as Li-ion cells [20]. In general, imaginary eigenvalues occur in diffusion-reaction systems when heat removal from the multilayer body can not keep up with the rate at which heat generation increases with temperature.

This work presents theoretical analysis of a diffusion-reaction problem in a two-dimensional multilayer body. The analysis accounts for general convective boundary conditions in the layered direction, whereas isothermal or adiabatic boundary conditions are considered in the other direction. An infinite series solution is derived, for which, the eigenequation is shown to be obtainable from the boundary and interface conditions. It is shown that under specific conditions, this problem may admit imaginary eigenvalues. Analysis of such imaginary eigenvalues is presented, including derivation of conditions in which thermal runaway may occur. In addition to improving the theoretical understanding of multilayer thermal conduction, the results from this work may also find practical application in improving the safety and reliability of engineering systems.

2. Mathematical modeling

Fig. 1 presents a schematic of a two-dimensional M-layer thermal transport problem with linear temperature-dependent heat generation/consumption in each layer. The reaction coefficient of each layer is denoted by β_m. Thickness of each layer is $x_m - x_{m-1}$ and the width of the body in the y direction is w. Thermal conductivity and diffusivity of each layer, assumed to be constant and uniform, are denoted by k_m and α_m, respectively. The multilayer body is exposed to general convective boundary conditions on either ends along the x direction. A non-zero initial temperature distribution is assumed in each layer. Under these assumptions, the differential equation governing the temperature field in each layer is given by

$$\alpha_m\left[\frac{\partial^2 T_m}{\partial x^2}+\frac{\partial^2 T_m}{\partial y^2}\right]+\beta_m T_m=\frac{\partial T_m}{\partial t}\,(\mathrm{m}=1,2,3\ldots\mathrm{M}) \tag{1}$$

The boundary and interface conditions in the x direction and initial conditions associated with Eq. (1) are given by

$$-k_1\frac{\partial T_1}{\partial x}+h_A T_1=0 \qquad (x=0) \tag{2}$$

$$k_M\frac{\partial T_M}{\partial x}+h_B T_M=0 \qquad (x=x_M) \tag{3}$$

$$T_m=T_{m+1} \qquad (x=x_m) \tag{4}$$

$$k_m\frac{\partial T_m}{\partial x}=k_{m+1}\frac{\partial T_{m+1}}{\partial x} \qquad (x=x_m) \tag{5}$$

$$T_m=T_{in,m}(x,y) \qquad (t=0) \tag{6}$$

Note that equations (4) and (5) represent perfect thermal contact and heat flux conservation, respectively, at interfaces between layers.

Non-dimensionalization is carried out based on the following:

$$\theta_m=\frac{T_m}{T_{ref}},\ \xi=\frac{x}{x_M},\ \eta=\frac{y}{x_M},\ \tau=\frac{\alpha_M t}{x_M^2},\ \gamma_m=\frac{x_m}{x_M},$$
$$\overline{w}=\frac{w}{x_M},\ \overline{k}_m=\frac{k_m}{k_M},\ \overline{\alpha}_m=\frac{\alpha_m}{\alpha_M},\ \overline{\beta}_m=\frac{\beta_m x_M^2}{\alpha_M},\ \theta_{in,m}=\frac{T_{in,m}}{T_{ref}},$$
$$Bi_A=\frac{h_A x_M}{k_M},\ Bi_B=\frac{h_B x_M}{k_M} \tag{8}$$

The non-dimensional set of equations is given by

$$\bar{\alpha}_m\left[\frac{\partial^2\theta_m}{\partial x^2}+\frac{\partial^2\theta_m}{\partial y^2}\right]+\bar{\beta}_m\theta_m=\frac{\partial\theta_m}{\partial\tau}\ (\mathrm{m}=1,2,3\ldots\mathrm{M}) \tag{9}$$

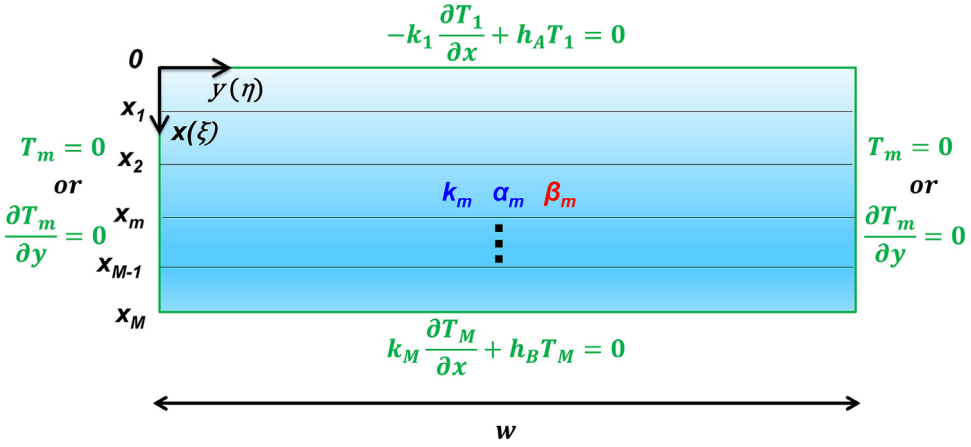

Fig. 1. Schematic of the two-dimensional multilayer diffusion-reaction problem considered here.

$$-\bar{k}_1\frac{\partial\theta_1}{\partial\xi}+Bi_A\theta_1=0 \qquad (\xi=0) \tag{10}$$

$$\frac{\partial\theta_M}{\partial\xi}+Bi_B\theta_M=0 \qquad (\xi=1) \tag{11}$$

$$\theta_m=\theta_{m+1} \qquad (\xi=\gamma_m) \quad (m=1,2..M-1) \tag{12}$$

$$\bar{k}_m\frac{\partial\theta_m}{\partial\xi}=\bar{k}_{m+1}\frac{\partial\theta_{m+1}}{\partial\xi} \qquad (\xi=\gamma_m) \quad (m=1,2..M-1) \tag{13}$$

$$\theta_m=\theta_{in,m}(\xi,\eta) \qquad (\tau=0) \tag{14}$$

Two separate cases corresponding to isothermal and adiabatic boundary conditions along the η boundaries are considered in the following sub-sections.

2.1. Isothermal conditions at the η boundaries

The first case considered here assumes isothermal conditions at the η boundaries. This is thermally the most favorable boundary condition for avoiding divergence of the temperature field due to the maximum capability of heat removal at these boundaries. In this case, the boundary conditions in the η direction may be written as

$$\theta_m=0 \text{ at } \eta=0 \quad (m=1,2..M) \tag{15a}$$

$$\theta_m=0 \text{ at } \eta=\bar{w} \quad (m=1,2..M) \tag{15b}$$

In order to solve this problem, the following separable form of the temperature distribution may be written

$$\theta_m(\xi,\eta,\tau)=f(\xi)u(\eta)g(\tau) \tag{16}$$

Substituting Eq. (16) into Eq. (9), a general solution for Eqs. (9)-(15) is expressed as follows

$$\begin{aligned}\theta_m(\xi,\eta,\tau)&=\sum_{n=1}^{\infty}\sum_{p=1}^{\infty}c_{n,p}[A_{m,n,p}\cos(\omega_{m,n,p}\xi)\\&+B_{m,n,p}\sin(\omega_{m,n,p}\xi)]\sin(\varepsilon_p\eta)\exp\left(-\lambda_{n,p}^2\tau\right)(m=1,2..M)\end{aligned} \tag{17}$$

In Eq. (17), $\varepsilon_p=\frac{p\pi}{\bar{w}}$ are the eigenvalues in the η-direction and $\omega_{m,n,p}$ are given by

$$\omega_{m,n,p}=\sqrt{\frac{\lambda_{n,p}^2+\bar{\beta}_m}{\bar{\alpha}_m}-\varepsilon_p^2} \quad (\mathrm{m}=1,2,3\ldots\mathrm{M}) \tag{18}$$

Note that the spatial eigenvalues $\lambda_{n,p}$ in the ξ direction depend on the spatial eigenvalues ε_p in the η direction – each ε_p generates one set of $\lambda_{n,p}$.

The initial condition, along with the principle of orthogonality of eigenfunctions is used to determine the coefficients $c_{n,p}$ in Eq. (17) as shown below

$$\begin{aligned}c_{n,p}=\frac{1}{N_{n,p}}\sum_{m=1}^{M}\frac{\bar{k}_m}{\bar{\alpha}_m}\int_{\gamma_{m-1}}^{\gamma_m}\int_0^{\bar{w}}\theta_{in,m}(\xi,\eta)[A_{m,n,p}\cos(\omega_{m,n,p}\xi)\\+B_{m,n,p}\sin(\omega_{m,n,p}\xi)]\sin(\varepsilon_p\eta)d\eta d\xi\end{aligned} \tag{19a}$$

where $\gamma_0=0$. The norms $N_{n,p}$ are obtained as follows

$$\begin{aligned}N_{n,p}=\sum_{m=1}^{M}\frac{\bar{k}_m}{\bar{\alpha}_m}\int_{\gamma_{m-1}}^{\gamma_m}\int_0^{\bar{w}}\theta_{in,m}(\xi,\eta)\\\{[A_{m,n,p}\cos(\omega_{m,n,p}\xi)\\+B_{m,n,p}\sin(\omega_{m,n,p}\xi)]\sin(\varepsilon_p\eta)\}^2d\eta d\xi\end{aligned} \tag{19b}$$

for each p and n, The unknowns $A_{m,n,p}$ and $B_{m,n,p}$ appearing in Eq. (17) satisfy $2M$ linear algebraic equations that may be obtained by inserting eq. (17) into the boundary and interfacial conditions given by Eqs. (10)–(13). In order to ensure a non-trivial solution of the problem, one must ensure that the determinant formed by the matrix of the coefficients of these equations must be zero, which results in the eigenequation for the problem. Further, due to redundancy, one may set $A_{1,n,p}$ to one and determine all other unknowns from the linear algebraic equations.

This is illustrated for the specific case of a two-layer body. One may obtain the following set of equations for the unknown coefficients $A_{1,n,p}$, $B_{1,n,p}$, $A_{2,n,p}$ and $B_{2,n,p}$

$$\begin{bmatrix} Bi_A & -\bar{k}_1\omega_{1,n,p} & 0 & 0\\ \cos(\omega_{1,n,p}\gamma_1) & \sin(\omega_{1,n,p}\gamma_1) & -\cos(\omega_{2,n,p}\gamma_1) & -\sin(\omega_{2,n,p}\gamma_1)\\ -\bar{k}_1\omega_{1,n,p}\sin(\omega_{1,n,p}\gamma_1) & \bar{k}_1\omega_{1,n,p}\cos(\omega_{1,n,p}\gamma_1) & \omega_{2,n,p}\sin(\omega_{2,n,p}\gamma_1) & -\omega_{2,n,p}\cos(\omega_{2,n,p}\gamma_1)\\ 0 & 0 & -Bi_B\cos(\omega_{2,n,p})+\omega_{2,n,p}\sin(\omega_{2,n,p}) & -Bi_B\sin(\omega_{2,n,p})-\omega_{2,n,p}\cos(\omega_{2,n,p}) \end{bmatrix}\begin{bmatrix}A_{1,n,p}\\B_{1,n,p}\\A_{2,n,p}\\B_{2,n,p}\end{bmatrix}=\begin{bmatrix}0\\0\\0\\0\end{bmatrix} \tag{20}$$

By setting the determinant of the matrix shown in Eq. (20) to zero, the following transcendental eigenequation for $\lambda_{n,p}$ may be

derived:

$$f(\lambda_{n,p}) = \bar{k}_1\omega_{1,n,p}\frac{-\bar{k}_1\omega_{1,n,p} + Bi_A\cot\omega_{1,n,p}\gamma_1}{\bar{k}_1\omega_{1,n,p}\cot\omega_{1,n,p}\gamma_1 + Bi_A} + \omega_{2,n,p}\frac{-\omega_{2,n,p} + Bi_B\cot\omega_{2,n,p}(1-\gamma_1)}{\omega_{2,n,p}\cot\omega_{2,n,p}(1-\gamma_1) + Bi_B} = 0 \quad (21)$$

Further, without loss of generality, $A_{1,n,p}$ is chosen to be equal to 1, based on which, all other coefficients are determined as follows:

$$B_{1,n,p} = \frac{Bi_A}{\bar{k}_1\omega_{1,n,p}} \quad (22)$$

$$A_{2,n,p} = \frac{\cos\omega_{1,n,p}\gamma_1 + \frac{Bi_A}{\bar{k}_1\omega_{1,n,p}}\sin\omega_{1,n,p}\gamma_1}{\cos\omega_{2,n,p}\gamma_1 + \sin\omega_{2,n,p}\gamma_1\frac{\omega_{2,n,p}\sin\omega_{2,n,p} - Bi_B\cos\omega_{2,n,p}}{\omega_{2,n,p}\cos\omega_{2,n,p} + Bi_B\sin\omega_{2,n,p}}} \quad (23)$$

$$B_{2,n,p} = A_{2,n,p}\frac{\omega_{2,n,p}\sin\omega_{2,n,p} - Bi_B\cos\omega_{2,n,p}}{\omega_{2,n,p}\cos\omega_{2,n,p} + Bi_B\sin\omega_{2,n,p}} \quad (24)$$

2.2. Adiabatic conditions at the η boundaries

In contrast with isothermal conditions at the η boundaries considered in section 2.1, an adiabatic condition is thermally the most unfavorable scenario, as it represents the least heat removal at the boundary, and therefore, the greatest likelihood of divergence in the temperature field. The problem statement for this problem is identical to the one in section 2.1, except for the following boundary conditions on the y boundaries instead of Eqs. (15a) and (15b)

$$\frac{\partial\theta_m}{\partial\eta} = 0 \qquad (\eta = 0)\ (m = 1, 2..M) \quad (25a)$$

$$\frac{\partial\theta_m}{\partial\eta} = 0 \qquad (\eta = \bar{w})\ (m = 1, 2..M) \quad (25b)$$

Using a similar approach as the previous section, a general solution for this case is presented as shown below

$$\theta_m(\xi,\tau) = \sum_{n=1}^{\infty}\sum_{p=0}^{\infty} c_{n,p}[A_{m,n,p}\cos(\omega_{m,n,p}\xi) + B_{m,n,p}\sin(\omega_{m,n,p}\xi)]\cos(\varepsilon_p\eta)\exp\left(-\lambda_{n,p}^2\tau\right)\ (m = 1, 2..M) \quad (26)$$

where the eigenvalues $\lambda_{n,p}$ and ε_p are the same as the isothermal problem in Section 2.1. Also note that unlike the solution for the isothermal problem, the summation in the η direction for this problem begins with $p = 0$ instead of $p = 1$, as was the case with the isothermal problem. The requirement to include the $p = 0$ eigenvalue for the adiabatic case arises because when both boundaries are adiabatic, then $\lambda = 0$ also satisfies the eigenequation, and, therefore, must be explicitly included [8].

The coefficients $c_{n,p}$ are obtained in a similar fashion as follows

$$c_{n,p} = \frac{1}{N_{n,p}}\sum_{m=1}^{M}\frac{\bar{k}_m}{\bar{\alpha}_m}\int_{\gamma_{m-1}}^{\gamma_m}\int_0^{\bar{w}}\theta_{in,m}(\xi,\eta)[A_{m,n,p}\cos(\omega_{m,n,p}\xi) + B_{m,n,p}\sin(\omega_{m,n,p}\xi)]\cos(\varepsilon_p\eta)d\eta d\xi \quad (27a)$$

In Eq. (27a), the norms $N_{n,p}$ are given by

$$N_{n,p} = \sum_{m=1}^{M}\frac{\bar{k}_m}{\bar{\alpha}_m}\int_{\gamma_{m-1}}^{\gamma_m}\int_0^{\bar{w}}\theta_{in,m}(\xi,\eta)\left\{[A_{m,n,p}\cos(\omega_{m,n,p}\xi) + B_{m,n,p}\sin(\omega_{m,n,p}\xi)]\cos(\varepsilon_p\eta)\right\}^2 d\eta d\xi \quad (27b)$$

Note that despite the identical eigenvalues for the isothermal and adiabatic cases, these cases are expected to behave very differently. This is because the adiabatic case includes one additional term corresponding to $p = 0$. This has a profound impact on the appearance of imaginary eigenvalues and thermal runaway, as discussed in Sections 3 and 4.5.

Due to the presence of the linear heat generation term, some of the eigenvalues of the problems described above may be imaginary, due to which, divergence in the temperature distribution at large times may be expected [15]. An imaginary eigenvalue analysis is presented in the next section. Results related to the impact of relevant problem parameters on temperature evolution and distribution are examined in the following section.

3. Imaginary eigenvalue analysis

In addition to the usual real eigenvalues, the analytical model derived in this work is also expected to result in multiple imaginary eigenvalues, similar to prior work on one-dimensional multilayer diffusion-reaction problems [15]. These imaginary eigenvalues have been shown to result in divergence of the temperature field at large times. In the present problem, two-dimensional case, there may be multiple imaginary eigenvalues in the ξ direction for each eigenvalue in the η direction. The number of imaginary eigenvalues corresponding to an eigenvalue in the η direction largely depends on the magnitude of the η eigenvalue, as well as reaction term coefficients, diffusivities and Biot numbers.

Since imaginary eigenvalues are associated with the thermal runaway phenomenon, which is of much practical interest, it is important to fully understand the nature of imaginary eigenvalues in the present 2D problem. Specifically, it is of much practical interest to derive expressions for the limiting conditions at which the temperature distribution does not diverge. This is presented here for a two-layer body. In order to do so, one may substitute $\hat{\lambda}_{n,p}^2 = -\lambda_{n,p}^2$ in equation (21), which results in the following eigenequation along the imaginary axis

$$f\left(\hat{\lambda}_{n,p}\right) = \bar{k}_1\hat{\omega}_{1,n,p}\frac{\bar{k}_1\hat{\omega}_{1,n,p} + Bi_A\coth\hat{\omega}_{1,n,p}\gamma_1}{\bar{k}_1\hat{\omega}_{1,n,p}\coth\hat{\omega}_{1,n,p}\gamma_1 + Bi_A} + \hat{\omega}_{2,n,p}\frac{\hat{\omega}_{2,n,p} + Bi_B\coth\hat{\omega}_{2,n,p}(1-\gamma_1)}{\hat{\omega}_{2,n,p}\coth\hat{\omega}_{1,n,p}(1-\gamma_1) + Bi_B} = 0 \quad (28)$$

where $\hat{\omega}_{m,n,p} = \sqrt{\frac{\hat{\lambda}_{n,p}^2 - \bar{\beta}_m}{\bar{\alpha}_m} + \varepsilon_p^2}$.

Due to the monotonically increasing nature of the eigenfunction, at least one imaginary eigenvalue exists if $f(\hat{\lambda} = 0) < 0$. Further, additional imaginary eigenvalue may exist if the eigenfunction attains an infinite value at one or more locations along the $\hat{\lambda}$ axis. It can be shown that this occurs if either of the following two equations are satisfied:

$$\bar{k}_1\hat{\omega}_{1,n,p}\coth\hat{\omega}_{1,n,p}\gamma_1 + Bi_A = 0 \quad (29)$$

$$\hat{\omega}_{2,n,p}\coth\hat{\omega}_{2,n,p}(1-\gamma_1) + Bi_B = 0 \quad (30)$$

Similar to recently presented analysis for a one-dimensional problem [21], the total number of imaginary eigenvalues expected for a given set of problem parameters of the two-dimensional problem may be shown to be given by $n_1 + n_2 + \delta$, where n_1 is the smallest non-negative integer for which $\bar{\beta}_1 - \bar{\alpha}_1\mu_{1,n_1+1}^2 - \varepsilon_p^2 < 0$, n_2 is the smallest non-negative integer for which $\bar{\beta}_2 - \mu_{2,n_2+1}^2 - \varepsilon_p^2 < 0$, and $\delta = 1$ if $f(0) < 0$ and $\delta = 0$ otherwise. Further, the condition for convergence, i.e., no imaginary eigenvalues at all, may be written simply as $n_1 + n_2 + \delta = 0$. Note that since there are multiple sets of eigenvalues $\lambda_{n,p}$ for different values of p, therefore, the condition for convergence must consider the most thermally unfavorable conditions, i.e., one must use $p = 1$ for the isothermal case.

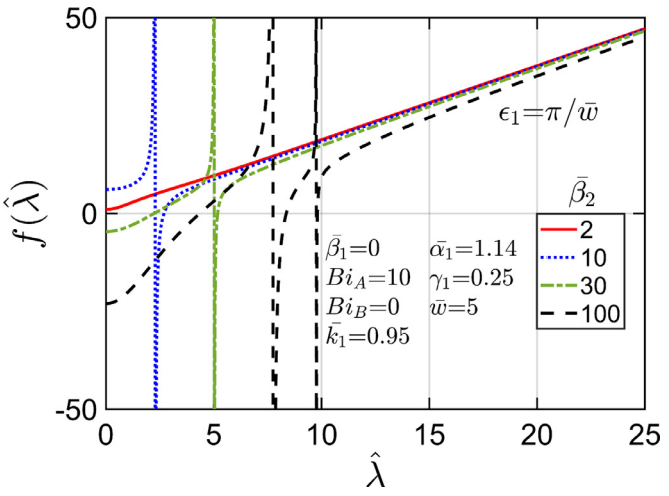

Fig. 2. Eigenfunction plot in imaginary space for $\bar{\beta}_2 = 2$, 10, 30, 100 and $p = 1$. Problem parameters are $\bar{\beta}_1 = 0$, $\bar{\alpha}_1 = 1.14$, $\bar{k}_1 = 0.95$, $\gamma_1 = 0.25$, $\bar{w} = 5$, $Bi_A = 10$ and $Bi_B = 0$.

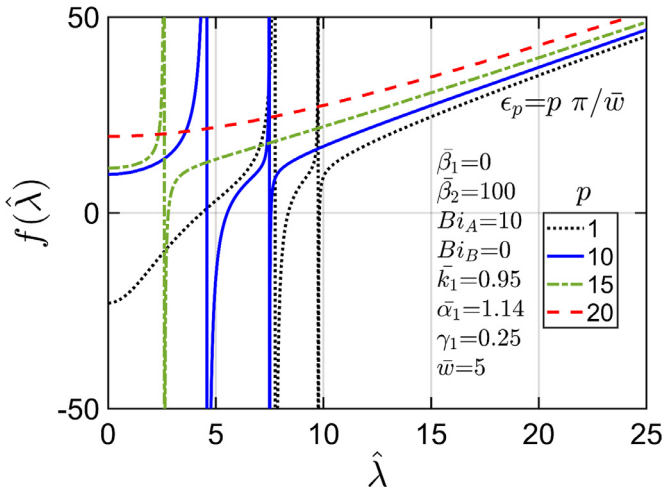

Fig. 3. Eigenfunction plot along the imaginary axis for p = 1,2,3,4. Problem parameters are $\bar{\beta}_1 = 0$, $\bar{\beta}_2 = 100$, $\bar{\alpha}_1 = 1.14$, $\bar{k}_1 = 0.95$, $\gamma_1 = 0.25$, $\bar{w} = 5$, $Bi_A = 10$ and $Bi_B = 0$.

In contrast, for the adiabatic case, the summation in the η direction begins at $p = 0$, and therefore, one must consider $p = 0$ in the conditions listed above. It can be easily seen that, because ε_p are an increasingly series of numbers, therefore, if the condition for convergence holds for the smallest possible value of p, it will also hold for all subsequent values as well.

For a representative set of parameters ($\bar{\beta}_1 = 0$, $\bar{\alpha}_1 = 1.14$, $\bar{k}_1 = 0.95$, $\gamma_1 = 0.25$, $\bar{w} = 5$, $Bi_A = 10$ and $Bi_B = 0$), the eigenfunction plot along the imaginary axis is presented in Fig. 2 for multiple values of $\bar{\beta}_2$. These plots correspond to the $p = 1$ eigenvalue in the η direction, i.e., $\varepsilon_1 = \frac{\pi}{\bar{w}}$. As the value of $\bar{\beta}_2$ goes up, the curves in Fig. 2 show, as expected, that the number and magnitude of imaginary eigenvalues increases. The physical interpretation of this observation is that divergence of the temperature field and the thermal runaway phenomena become more and more severe as the value of the reaction coefficient increases. This is also consistent with the analysis of number of imaginary eigenvalues presented above, where it can be seen that as $\bar{\beta}_2$ increases, both n_1 and n_2 increase, resulting in a greater number of imaginary eigenvalues. Plots such as Fig. 2 can be of practical use by predicting the occurrence and severity of thermal runaway for a given set of conditions. Despite the inherent simplification in the linearized modeling of the reaction term here, imaginary eigenvalue analysis is of much practical use, since the value of $\bar{\beta}_2$ can be correlated to practical parameters, such as reaction rates and Arrhenius parameters for the decomposition reactions responsible for thermal runaway in a Li-ion cell [22].

Figure 3 illustrates the impact of the η direction eigenvalue on the number of imaginary eigenvalues encountered. With the same set of problem parameters as prior, Fig. 3 plots the eigenfunction along the imaginary axis for different values of p, with $\varepsilon_p = \frac{n\pi}{\bar{w}}$. These plots clearly show that the number of imaginary eigenvalues decrease as the magnitude of ε_p increases. For $p = 20$, no imaginary eigenvalues are encountered at all. These observations are consistent with the discussion above, since increasing the value of p increases ε_p, which reduces the values of n_1 and n_2 by making the criteria for convergence easier to achieve.

Finally, the effect of Biot number on the number of imaginary eigenvalues is presented in Fig. 4, which plots the eigenfunction in the imaginary space for two different values of the Biot number, assumed to be the same at both ends. Two different cases with $\bar{\beta}_2 = 100$ and $\bar{\beta}_2 = 10$ are presented in Figs. 4(a) and 4(b), respectively. For a large reaction coefficient, such as in Fig. 4(a), increasing the value of the Biot number results in a reduction in the number of imaginary eigenvalues, but does not completely eliminate it. This is because even an isothermal boundary that removes the most possible heat is not able to overcome the large heat generation due to large $\bar{\beta}_2$. In this case, therefore, divergence occurs regardless of the value of the Biot number. On the other hand, when the reaction coefficient is not as large, such as in Fig. 4(b), increasing the value of the Biot number results in elimination of the imaginary eigenvalue, and, at a value of 50, the eigenfunction curve monotonically increases and never crosses the x axis. Note that further increasing the value of the Biot number does not produce significant change in the curves in either plot, indicating that a value of Biot number of 50 is already quite close to the limiting condition of isothermal boundary condition.

4. Results and discussion

4.1. Model verification by comparison with numerical simulations

The analytical models presented in sections 2.1 and 2.2 are verified by comparison with finite-element based numerical simulations carried out in ANSYS-CFX. For the specific case of adiabatic conditions at the η boundaries, Fig. 5 presents this comparison in the context of a two-layer body, where temperature is plotted across the layers at $\eta = 2.5$ and at multiple times in Fig. 5(a) and at $\xi = 0.625$ as a function of η in Fig. 5(b). In addition, temperature at the center of both layers is plotted as a function of time in Fig. 5(c). Problem parameters are $\bar{\beta}_1 = 0$, $\bar{\beta}_2 = 30$, $\bar{\alpha}_1 = 1.14$, $\bar{k}_1 = 0.95$, $\gamma_1 = 0.25$, $\bar{w} = 5$, $Bi_A = 10$ and $Bi_B = 0$. The values of thermal properties are based on a Li-ion cell covered by a Polytetrafluoroethylene (PTFE) insulating material. While the properties of these materials vary in a wide range, representative values for a Li-ion cell are taken based on past work [23], whereas values for PTFE are chosen from available databases. In the case of a cell covered by insulation material on both sides, consideration of only half the geometry by symmetry results in adiabatic conditions on one end. The initial condition is a temperature of 1 between $\eta = 0.4\bar{w}$ and $\eta = 0.6\bar{w}$ in layer 2, and zero elsewhere. This initial condition is assumed throughout this work, unless specified otherwise. Due to the relatively large value of $\bar{\beta}_2$, the temperature field in this problem diverges at large times. Nevertheless, there is excellent agreement between the analytical model and numerical simulations, as shown in Figs. 5(a)-(c).

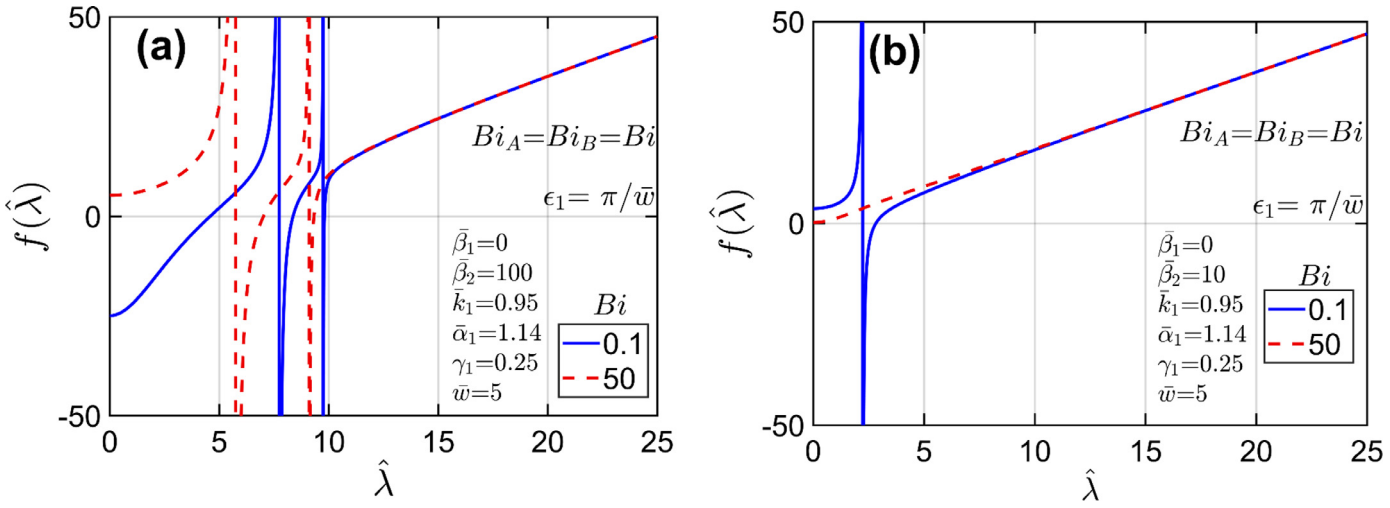

Fig. 4. Eigenfunction plot in imaginary space for $Bi = 0.1$, 50 and $\varepsilon_1 = \frac{\pi}{\bar{w}}$. (a) $\bar{\beta}_2 = 100$, (b) $\bar{\beta}_2 = 10$. Other problem parameters are $\bar{\beta}_1 = 0$, $\bar{\beta}_2 = 100$, $\bar{\alpha}_1 = 1.14$, $\bar{k}_1 = 0.95$, $\gamma_1 = 0.25$, $\bar{w} = 5$. Conditions at the η boundaries are adiabatic.

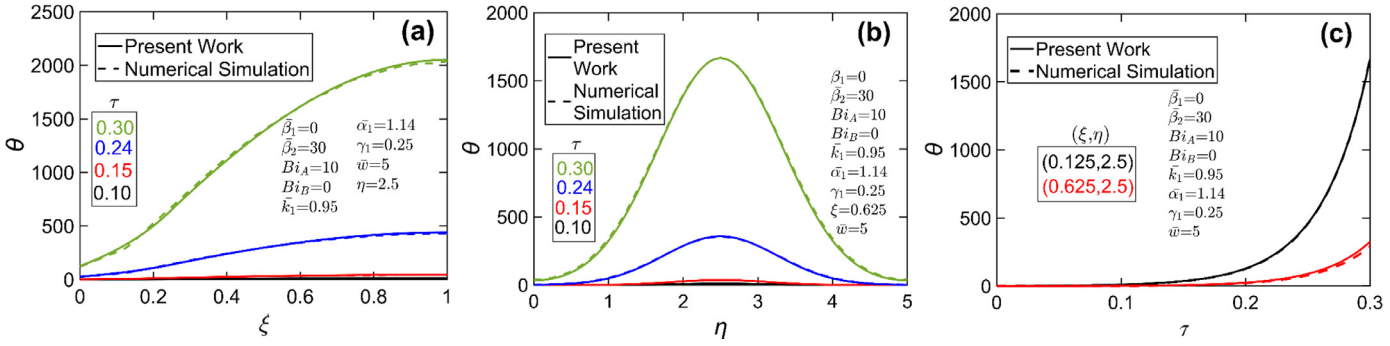

Fig. 5. Comparison of present work with numerical simulations for a case where the temperature field diverges at large times: (a) θ vs ξ at $\eta = \bar{w}/2$ and multiple times, (b) θ vs η at $\xi = 0.625$ and at multiple times, (c) θ vs τ at the center of layers 1 and 2. Problem parameters are $\bar{\beta}_1 = 0$, $\bar{\beta}_2 = 30$, $\bar{\alpha}_1 = 1.14$, $\bar{k}_1 = 0.95$, $\gamma_1 = 0.25$, $\bar{w} = 5$, $Bi_A = 10$ and $Bi_B = 0$, with adiabatic boundaries in the η direction.

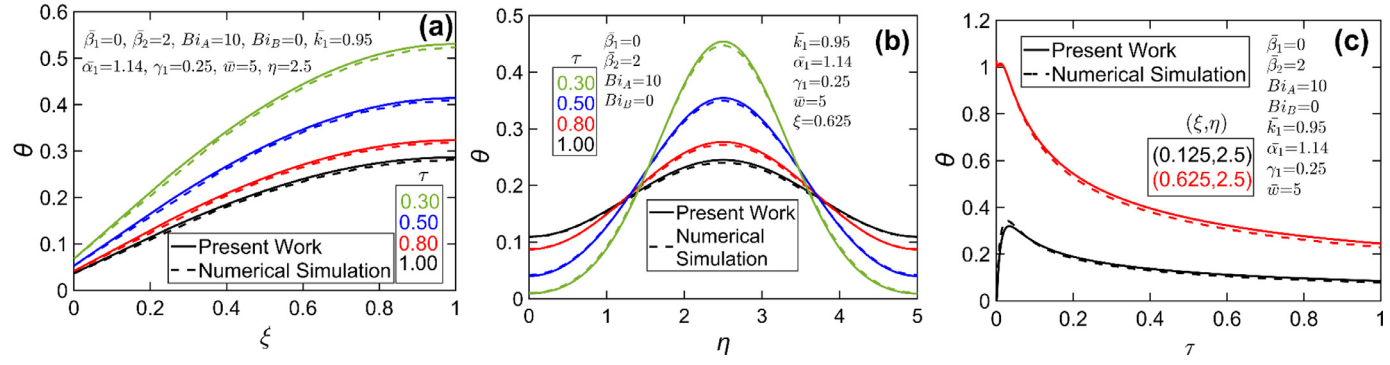

Fig. 6. Comparison of present work with numerical simulations for a case where the temperature field converges at large times: (a) θ vs ξ at $\eta = \bar{w}/2$ and multiple times, (b) θ vs η at $\xi = 0.625$ and at multiple times, (c) θ vs τ at the center of layers 1 and 2. Problem parameters are $\bar{\beta}_1 = 0$, $\bar{\beta}_2 = 2$, $\bar{\alpha}_1 = 1.14$, $\bar{k}_1 = 0.95$, $\gamma_1 = 0.25$, $\bar{w} = 5$, $Bi_A = 10$ and $Bi_B = 0$, with adiabatic boundaries in the η direction.

A similar comparison with numerical simulations is presented in Fig. 6 for a case where the reaction coefficient in the second layer is much lower, $\bar{\beta}_2 = 2$. Other parameters are identical to Fig. 5. Similar to Fig. 5, there is excellent agreement in this converging case, with a reasonably low worst-case deviation of 7%.

Note that the accuracy of infinite series solutions such as those derived in this work depends critically on the number of eigenvalues considered. In this work, a maximum value of 50 is used for n and p in the summations in equations (17) and (26). It is verified through a convergence analysis that consideration of additional eigenvalues does not significantly alter the computed temperature distribution. Whenever appropriate, a set of one or more imaginary eigenvalues are also computed and included in the solution.

4.2. Typical temperature maps

Figures 7 and 8 present two-dimensional temperature distributions for a two-layer body with the same problem parameters as Figs. 5 and 6, respectively. In the first case, the large value of

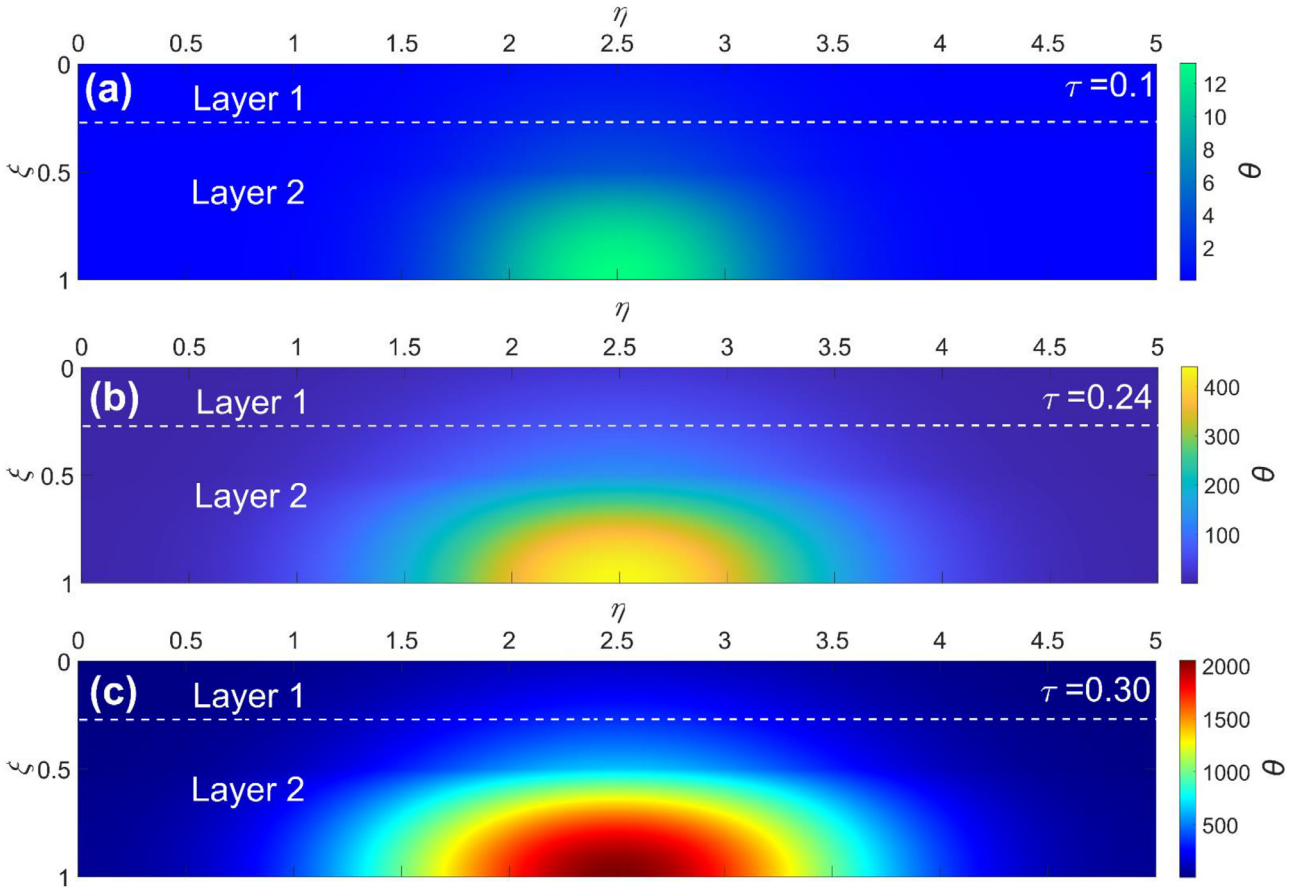

Fig. 7. Temperature colormaps in the entire geometry at (a) $\tau = 0.1$, (b) $\tau = 0.15$, (c) $\tau = 0.24$ for a case in which the temperature field diverges at large times. Problem parameters are identical to Figure 5.

the reaction coefficient results in divergence due to excessive heat generated compared to dissipation at the boundaries. Temperature colormaps at multiple times for this case plotted in Fig. 7 clearly show that divergence first occurs in the middle region of the two-layer body closer to $\xi = 1$, which is consistent with the adiabatic nature of that boundary and the nature of the initial temperature distribution. On the other hand, in Fig. 8, which corresponds to $\bar{\beta}_2 = 2$, the convective boundary condition is strong enough to dissipate heat generated in layer 2, and therefore, the temperature field converges at large times, despite the positive value of $\bar{\beta}_2$. As discussed in section 3, the divergence in Fig. 7 is mathematically explained on the basis of the presence of imaginary eigenvalues in the solution. In contrast, all eigenvalues for the problem shown in Fig. 8 are real, and therefore, the temperature field converges at large times.

4.3. Impact of width

The impact of width $\bar{w}$ on the temperature field is investigated in Fig. 9. Temperature at the midpoint of layer 2 ($\xi = \frac{1+\gamma_1}{2}, \eta = \bar{w}/2$) is plotted as a function of time for isothermal and adiabatic conditions at the η boundaries in Fig. 9(a) and 9(b), respectively. In each case, curves corresponding to two different widths are presented. All parameters are identical to ones used in preceding figures, except $\bar{\beta}_2 = 5$. Fig. 9(a) shows that while divergence occurs for $\bar{w} = 5$, bringing the isothermal walls closer to each case in the $\bar{w} = 1$ case results in sufficiently enhanced heat removal, so that there is no divergence in temperature for this case. Mathematically, as $\bar{w}$ is reduced, the total number of imaginary eigenvalues encountered also reduces. In general, the regions surrounding the central region with high initial temperature act as a heat sink at small times, which is why there is a dip in the curves in Fig. 9(b) at small times. However, as the temperature of these regions begin to rise due to heat generation, the impact of insufficient heat removal begins to dominate, resulting in increase in temperature at the midpoint after an initial decline. Only in the case of isothermal walls with $\bar{w} = 1$ does the close presence of a heat-dissipating boundary overcome heat generation, and causes the temperature to go down monotonically.

Mathematically, divergence is caused by the appearance of imaginary eigenvalues in the solution of these problems. In Fig. 9, the isothermal problem with $\bar{w} = 1$ is the only case with no imaginary eigenvalues. Note that even though the eigenvalues $\lambda_{n,p}$ and ε_p are identical for the isothermal and adiabatic problems, the adiabatic problem contains an additional series of $\lambda_{n,p}$, corresponding to $p = 0$, which leaves open the possibility of appearance of imaginary eigenvalues and divergence, even when, for the same set of parameters, the isothermal problem converges.

4.4. Effect of the reaction coefficient and ξ boundary conditions

Figs. 10(a) and 10(b) plot temperature at the midpoint in layer 2 as a function of time for multiple values of $\bar{\beta}_2$. Figs. 10(a) and 10(b) plots the temperature curves for relatively low and high values of $Bi_A = 0.1$ and $Bi_A = 10$, respectively. Adiabatic boundaries are assumed in the η direction. Other problem parameters are the same as Fig. 5. As expected, in Fig. 10(b), the temperature field converges for small values of $\bar{\beta}_2$ and diverges as the value of $\bar{\beta}_2$ increases. In contrast, the curves in Fig. 10(a) diverge for even small values of $\bar{\beta}_2$, which may be attributed to insufficient heat removal from

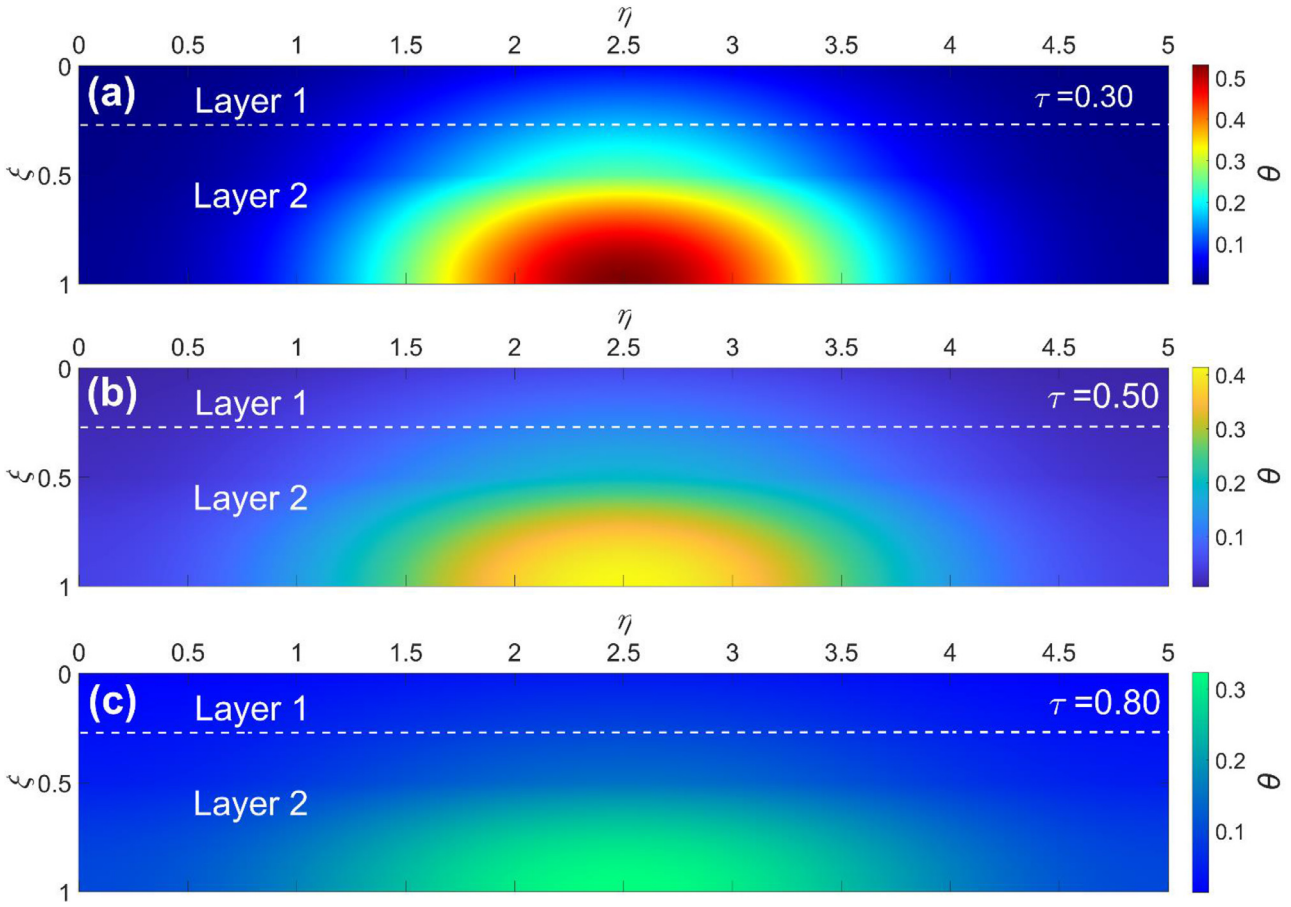

Fig. 8. Temperature colormaps in the entire geometry at (a) $\tau = 0.3$, (b) $\tau = 0.5$, (c) $\tau = 0.8$ for a case in which the temperature field converges at large times. Problem parameters are identical to Figure 6.

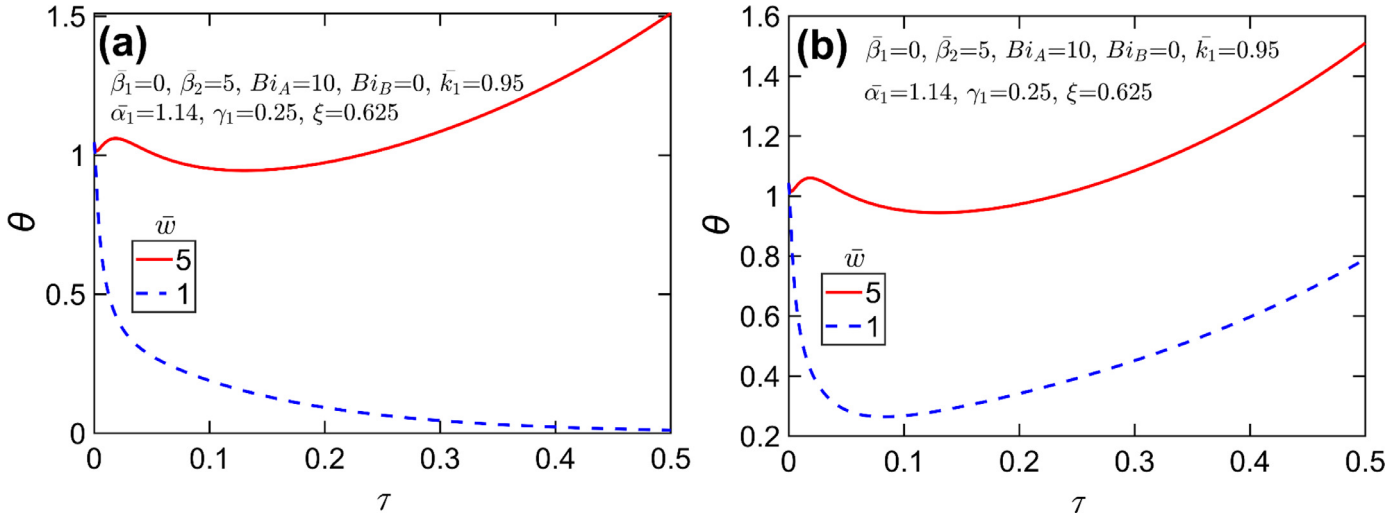

Fig. 9. Impact of $\bar{w}$ on temperature: θ vs τ in the middle of layer 2 for (a) isothermal, and (b) adiabatic conditions at the η boundaries. Problem parameters are $\bar{\beta}_1 = 0$, $\bar{\beta}_2 = 5$, $\bar{\alpha}_1 = 1.14$, $\bar{k}_1 = 0.95$, $\gamma_1 = 0.25$, $Bi_A = 10$ and $Bi_B = 0$.

the boundaries due to the small value of Bi_A. On the other hand, the Biot number in Fig. 10(b) is sufficiently large enough to ensure convergence for small values of $\bar{\beta}_2$. These plots allude to the existence of a threshold values of the reaction coefficient and Biot numbers that separates convergence and divergence of the temperature field.

A similar analysis of the impact of the ξ boundary conditions is presented in Fig. 11. Temperature as a function of time at the midpoint of layer 2 is plotted in Figs. 11(a) and 11(b), respectively, for four different values of Bi_A. Fig. 11(a) is used to analyze this problem for a small value of $\bar{\beta}_2 = 3$, whereas Fig. 11(b) presents similar plots for relatively higher value of $\bar{\beta}_2 = 5$. All other parameters are the same as Fig. 10. A large value of Bi_A corresponds to greater heat dissipation capability at $\xi = 0$. In Fig. 11(b), as Bi_A is increased, it can be clearly seen that the rate of divergence reduces significantly, but divergence is not prevented altogether. On

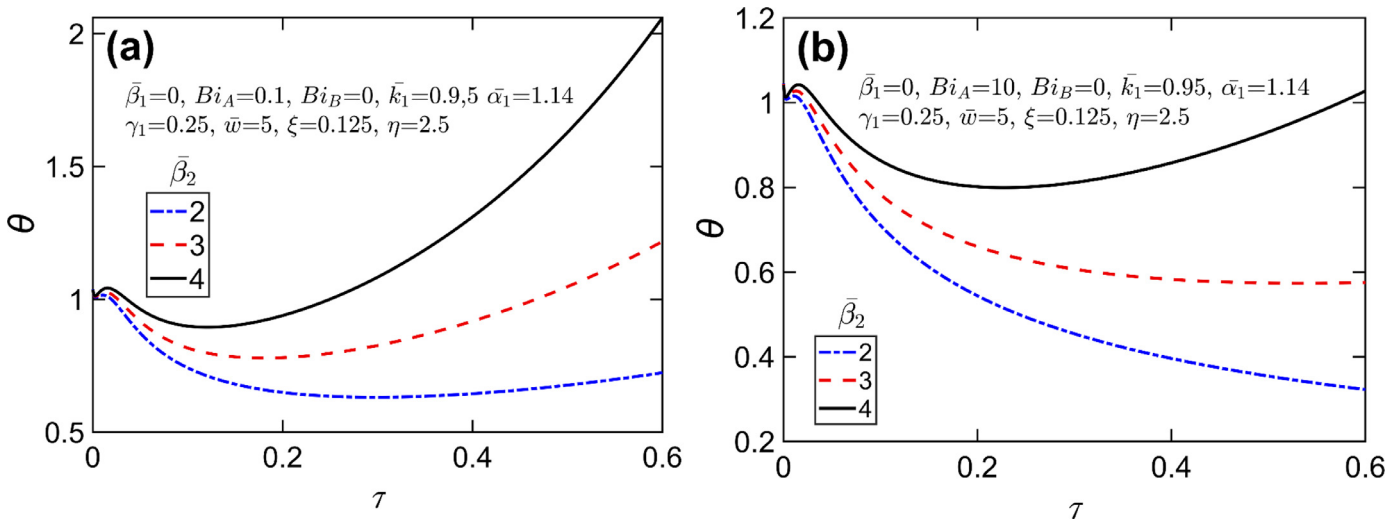

Fig. 10. Impact of $\bar{\beta}_2$ on temperature: θ vs τ in the middle of layer 2 for (a) $Bi_A = 0.1$, (b) $Bi_A = 10$. Problem parameters are $\bar{\beta}_1 = 0$, $\bar{\alpha}_1 = 1.14$, $\bar{k}_1 = 0.95$, $\gamma_1 = 0.25$, $\bar{w} = 5$ and $Bi_B = 0$. Adiabatic boundaries are assumed in the η direction.

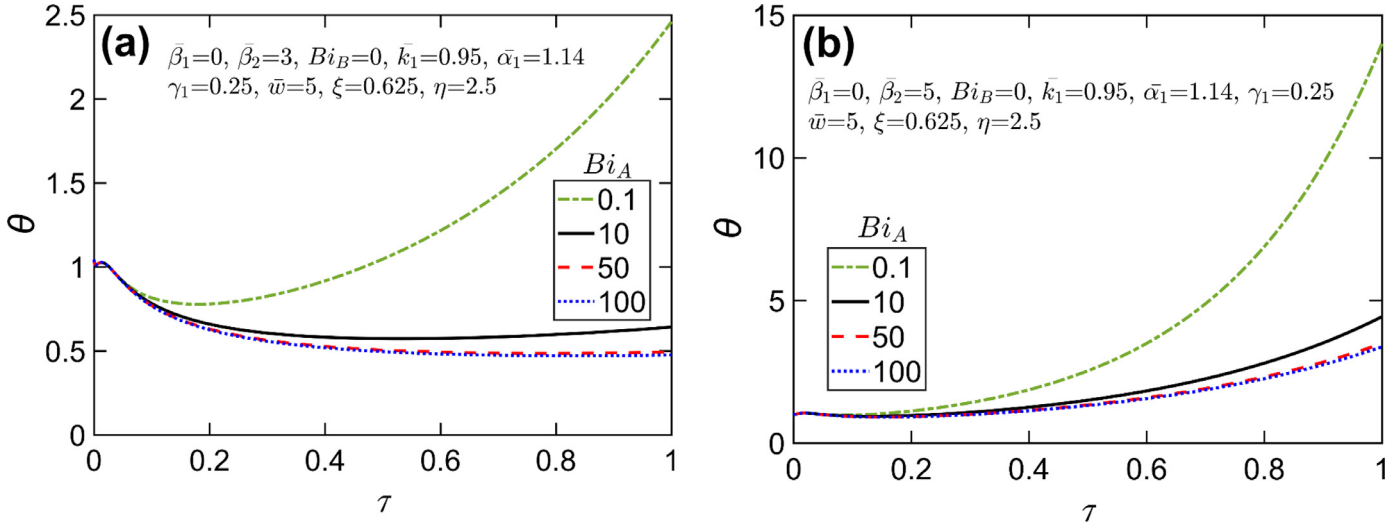

Fig. 11. Impact of Bi_A on temperature: θ vs τ in the middle of layer 2 for (a) $\bar{\beta}_2 = 3$, (b) $\bar{\beta}_2 = 5$. Problem parameters are $\bar{\beta}_1 = 0$, $\bar{\alpha}_1 = 1.14$, $\bar{k}_1 = 0.95$, $\gamma_1 = 0.25$, $\bar{w} = 5$ and $Bi_B = 0$.

the other hand, in Fig. 11(a), the temperature starts to converge as Bi_A is increased, as expected, due to greater heat dissipation rate.

4.5. Practical application: Thermal Runaway prediction in a Li-ion cell

The analytical models presented in section 2 are used to analyze thermal runaway in a practical problem. A prismatic Li-ion cell covered by Polytetrafluoroethylene (PTFE), a commonly used insulating material is considered. Based on previously reported thermal properties of the Li-ion cell [23], $\bar{\alpha}_1 = 1.21$ and $\bar{k}_1 = 0.80$ are assumed. In addition, the cell and PTFE are assumed to be of equal thickness ($\gamma_1 = 0.5$). There is no heat generation in the passive PTFE layer. By symmetry, the boundary at the cell end is taken to be adiabatic, i.e., $Bi_A = 0$. The two remaining problem parameters are the reaction coefficient in the cell, $\bar{\beta}_1$ and Biot number on the PTFE end, Bi_B. It is of interest to determine the regions in the $Bi_B - \bar{\beta}_1$ parameter space where thermal runaway may not occur. In order to do so, the number of imaginary eigenvalues are computed in this space, and the region with zero imaginary eigenvalues is identified as the converging region. Fig. 12(a) shows the curve that separates the converging and diverging regions for isothermal and adiabatic conditions in the η direction for $\bar{w} = 1$. Similar curves for a much wider geometry, $\bar{w} = 10$ are presented in Fig. 12(b). In these plots, regions below and above each curve correspond to convergence and divergence, respectively. These Figures show that, in general, the greater the value of Bi_B, the greater is the value of $\bar{\beta}_1$ that may be tolerated without divergence. As Bi_B increases, the maximum value of $\bar{\beta}_1$ increases slowly at first, due to poor heat dissipation at the PTFE end, and then increases more rapidly, as heat dissipation improves. Eventually, as Bi_B becomes very large, approaching isothermal conditions, the curves plateaus out, because further increase in Bi_B does not significantly improve heat removal since Bi_B is already quite large. The isothermal curve in Fig. 12(a) is much higher than the adiabatic curve, i.e., the converging region is much greater, because isothermal conditions result in much greater heat removal than adiabatic conditions. In contrast, these curves are much closer to each other for the case of $\bar{w} = 10$ case. This is because when the geometry is very wide, the influence of the η boundaries is relatively weaker, which is why the nature of η does not significantly impact convergence/divergence of the system.

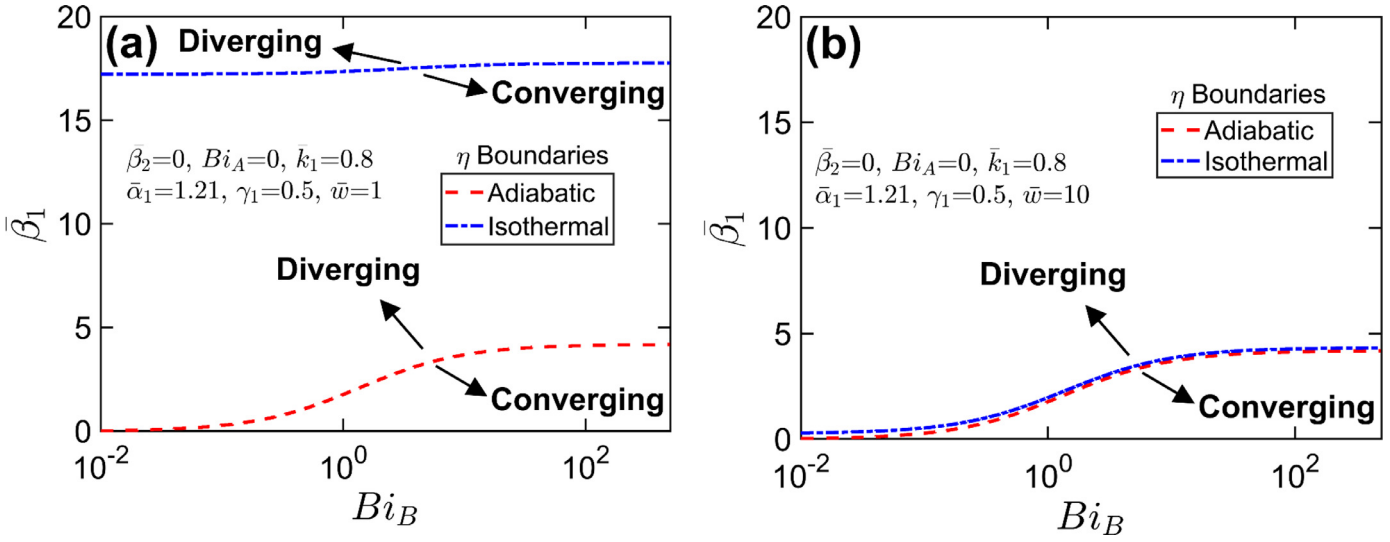

Fig. 12. Practical application of the theoretical model: Converging and diverging regions in the $Bi_B - \bar{\beta}_1$ space for a prismatic Li-ion cell covered by a PTFE layer for (a) $\bar{w} = 1$, and (b) $\bar{w} = 10$. Curves are shown for adiabatic and isothermal conditions on the η boundaries. Based on material properties and symmetry considerations, other problem parameters are $\bar{\beta}_2 = 0$, $Bi_B = 0$, $\bar{k}_1 = 0.8$, $\bar{\alpha}_1 = 1.21$, $\gamma_1 = 0.5$.

The curves presented in Fig. 12(a) and 12(b) may be used to identify safe and unsafe regions in the design of a practical Li-ion battery pack with the effect of the commonly used insulation plate accounted for.

5. Conclusions

The key novelty of the analysis presented in this work is in accounting for the reaction term in multilayer multidimensional heat and mass transfer problems that may occur in practical engineering systems, such as Li-ion cells. This is an improvement over the existing literature, where most such analysis is presented in the context of a one-dimensional body. While the consideration of the second dimension is clearly more complicated, it is also more realistic and accurate for practical engineering systems. The accounting of the reaction term in this work is shown to result in the possibility of imaginary eigenvalues. In addition to the theoretical interest in imaginary eigenvalues, these are also of much practical importance, due to the divergence in temperature field at large times caused by an imaginary eigenvalue. This corresponds to the thermal runaway phenomenon, the prediction and prevention of which is of much interest in the context of Li-ion cells and electrochemical energy storage.

While this work is presented in the context of a two-dimensional body, extension to three dimensions is straightforward, as it simply introduces an additional series of eigenfunctions to account for. A key limitation of the present work is that the boundary conditions in the y direction are assumed to be either isothermal or adiabatic. While these may be used to model specific heat/mass transfer scenarios, a more general treatment in the form of a convective boundary condition would be desirable. Unfortunately, however, the derivation of an eigenequation common to all layers in the x direction is possible only for isothermal or adiabatic boundaries.

While most of the plots presented here pertain to a two-layer body, the results are general enough that the thermal behavior of bodies with more than two layers can be easily computed as well. Finally, it is important to note that while this work is presented in the context of heat transfer, similar results apply for mass transfer problems as well. Such problems may occur, for example, in porous media mass transfer, reacting systems and electrochemistry. The generalized analysis of diffusion-reaction problems in a multilayer two-dimensional body presented here may be of practical importance in a variety of such engineering systems.

Declaration of Competing Interest

All authors declare that they do not have conflicts of interest as described by Elsevier's policies.

CRediT authorship contribution statement

Girish Krishnan: Methodology, Formal analysis, Validation, Investigation, Data curation, Writing – original draft, Writing – review & editing. **Ankur Jain:** Conceptualization, Methodology, Formal analysis, Validation, Investigation, Data curation, Supervision, Project administration, Writing – original draft, Writing – review & editing.

Data availability

Data will be made available on request.

Acknowledgments

This material is based upon work supported by CAREER Award No. CBET-1554183 from the National Science Foundation.

References

[1] L. Choobineh, A. Jain, An explicit analytical model for rapid computation of temperature field in a three-dimensional integrated circuit (3D IC), Int. J. Therm. Sci. 87 (2015) 103–109, doi:10.1016/j.ijthermalsci.2014.08.012.
[2] K. Daryabeigi, Thermal Analysis and Design Optimization of Multilayer Insulation for Reentry Aerodynamic Heating, J. Spacecraft Rockets 39 (2002) 509–514, doi:10.2514/2.3863.
[3] S.M. Becker, Analytic one-dimensional transient conduction into a living perfuse/non-perfuse two layer composite system, Heat Mass Transfer 48 (2012) 317–327, doi:10.1007/s00231-011-0886-5.
[4] A. Jain, S. McGinty, G. Pontrelli, Theoretical Modeling of Endovascular Drug Delivery into a Multilayer Arterial Wall from a Drug-Coated Balloon, Int. J. Heat Mass Transfer 187 (2022) 122572, doi:10.1016/j.ijheatmasstransfer.2022.122572.
[5] L. Ferragut, M.I. Asensio, J.M. Cascón, D. Prieto, J. Ramírez, An efficient algorithm for solving a multi-layer convection–diffusion problem applied to air pollution problems, Adv. Eng. Software 65 (2013) 191 –199, doi:10.1016/j.advengsoft.2013.06.010.
[6] H. French, Heat Transfer and Fluid Flow in Nuclear Systems, 1st, Pergamon Press, 1981 ISBN: 978-1483118369.

[7] A. Jain, M. Parhizi, L. Zhou, Multilayer One-Dimensional Convection-Diffusion-Reaction (CDR) Problem: Analytical Solution and Imaginary Eigenvalue Analysis, Int. J. Heat Mass Transfer 177 (2021) 121465, doi:10.1016/j.ijheatmasstransfer.2021.121465.
[8] D.W. Hahn, M.N. Özışık, Heat Conduction, Wiley, Hoboken, N.J., 2012. ISBN: 978-0470902936.
[9] M.D. Mikhailov, M.N. Özişik, Unified Analysis and Solutions of Heat and Mass Diffusion, Dover Publications, 1984 ISBN: 978-0486678764.
[10] M.R. Rodrigo, A.L. Worthy, Solution of multilayer diffusion problems via the Laplace transform, J. Mathemat. Analysis & Appl. 444 (2016) 475 –502, doi:10.1016/j.jmaa.2016.06.042.
[11] M. Parhizi, G. Kilaz, J. Ostanek, A. Jain, Analytical solution of the Convection-Diffusion-Reaction-Source (CDRS) equation using Green's function technique, Int. Communic. Heat Mass Transfer 131 (2022) 105869, doi:10.1016/j.icheatmasstransfer.2021.105869.
[12] A. Haji-Sheikh, J.V. Beck, Temperature solution in multi-dimensional multi-layer bodies, Int. J. Heat Mass Transfer 45 (2002) 1865–1877, doi:10.1016/S0017-9310(01)00279-4.
[13] H. Salt, Transient conduction in a two-dimensional composite slab—II. Physical interpretation of temperature modes, Int. J. Heat Mass Transfer 26 (1983) 1617–1623, doi:10.1016/S0017-9310(83)80081-7.
[14] M.D. Mikhailov, M.N. Özışık, Transient conduction in a three-dimensional composite slab, Int. J. Heat Mass Transfer 29 (1986) 340 –342, doi:10.1016/0017-9310(86)90242-5.
[15] A. Jain, M. Parhizi, L. Zhou, G. Krishnan, Imaginary Eigenvalues in Multi-layer One-Dimensional Thermal Conduction Problem with Linear Temperature-Dependent Heat Generation, Int. J. Heat Mass Transfer 170 (2021) 120993, doi:10.1016/j.ijheatmasstransfer.2021.120993.
[16] R. Chiba, An Analytical Solution for Transient Heat Conduction in a Composite Slab with Time-Dependent Heat Transfer Coefficient, Mathematical Problems in Engineering 4707860 (2018) 1–11, doi:10.1155/2018/4707860.
[17] L. Zhou, A. Jain, M. Parhizi, Temperature distribution in a multi-layer cylinder with circumferentially-varying convective heat transfer boundary conditions, Int. J. Therm. Sci. 160 (2021) 106673, doi:10.1016/j.ijthermalsci.2020.106673.
[18] L. Zhou, A. Jain, M. Parhizi, Theoretical modeling of heat transfer in a multi-layer rectangular body with spatially-varying convective heat transfer boundary condition, Int. J. Therm. Sci. 170 (2021) 107156, doi:10.1016/j.ijthermalsci.2021.107156.
[19] A. Jain, S. McGinty, G. Pontrelli, L. Zhou, Theoretical model for diffusion-reaction based drug delivery from a multilayer spherical capsule, Int. J. Heat Mass Transfer 183 (2022) 122072, doi:10.1016/j.ijheatmasstransfer.2021.122072.
[20] K. Shah, D. Chalise, A. Jain, Experimental and theoretical analysis of a method to predict thermal runaway in Li-ion cells, J. Power Sources 330 (2016) 167–174, doi:10.1016/j.jpowsour.2016.08.133.
[21] G. Krishnan, A. Jain, Derivation of Multiple but Finite Number of Imaginary Eigenvalues for Multilayer Diffusion-Reaction Problems, Int. J. Heat Mass Transfer 194 (2022) 123037, doi:10.1016/j.ijheatmasstransfer.2022.123163.
[22] I. Esho, K. Shah, A. Jain, Measurements and modeling to determine the critical temperature for preventing thermal runaway in Li-ion cells, Appl. Therm. Eng. 145 (2018) 287–294, doi:10.1016/j.applthermaleng.2018.09.016.
[23] S. Drake, D.A. Wetz, J.K. Ostanek, S.P. Miller, J.M. Heinzel, A. Jain, Measurement of anisotropic thermophysical properties of cylindrical Li-ion cells, J. Power Sources 252 (2014) 298–304, doi:10.1016/j.jpowsour.2013.11.107.